ACS central science

Research Article

Cite This: ACS Cent. Sci. 2018, 4, 1503−1510

http://pubs.acs.org/journal/acscii

pH Dependence of Zika Membrane Fusion Kinetics Reveals an Off-Pathway State

Robert J. Rawle,[†,#] Elizabeth R. Webster,[‡,#] Marta Jelen,[†] Peter M. Kasson,[*,†,§] and Steven G. Boxer[*,‡]

[†]Departments of Molecular Physiology and Biological Physics and of Biomedical Engineering, University of Virginia, Charlottesville, Virginia 22908, United States

[‡]Department of Chemistry, Stanford University, Stanford, California 94305, United States

[§]Science for Life Laboratory, Department of Cell and Molecular Biology, Uppsala University, Uppsala, Sweden 75124

Supporting Information

ABSTRACT: The recent spread of Zika virus stimulated extensive research on its structure, pathogenesis, and immunology, but mechanistic study of entry has lagged behind, in part due to the lack of a defined reconstituted system. Here, we report Zika membrane fusion measured using a platform that bypasses these barriers, enabling observation of single-virus fusion kinetics without receptor reconstitution. Surprisingly, target membrane binding and low pH are sufficient to trigger viral hemifusion to liposomes containing only neutral lipids. Second, although the extent of hemifusion strongly depends on pH, hemifusion rates are relatively insensitive to pH. Kinetic analysis shows that an off-pathway state is required to capture this pH-dependence and suggests this may be related to viral inactivation. Our surrogate-receptor approach thus yields new understanding of flaviviral entry mechanisms and should be applicable to many emerging viruses.

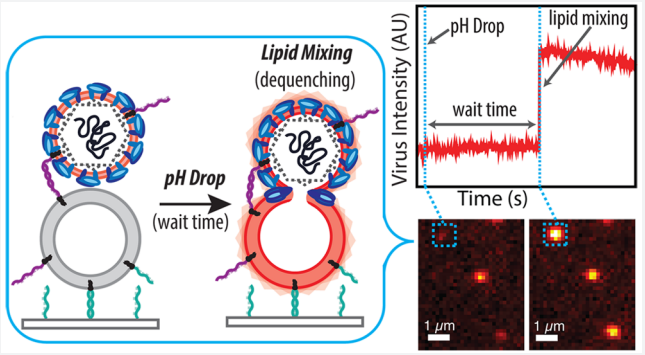

INTRODUCTION

Zika virus, an enveloped flavivirus, has recently emerged as a global health concern, causing febrile illness and congenital abnormalities.[1−4] It is a positive-sense, single-stranded RNA virus that is primarily transmitted to humans from *Aedes* mosquitos. Because Zika has only recently received much scientific study, its entry and fusion processes remain largely uncharacterized but are important both for scientific understanding and as possible targets for therapeutic intervention.

Currently, the entry and fusion of Zika are mostly understood by analogy to closely related flaviviruses such as dengue virus and West Nile virus. To infect a host cell, these viruses first bind to a receptor on the host cell surface. The virus is then internalized by endocytosis, and, as the endosome matures, its internal pH drops. This triggers a dramatic rearrangement in the viral E-proteins, which mediate fusion with the endosomal membrane, allowing the viral RNA to enter the cell.[5−8] Several factors in addition to low pH, such as endosomal lipid composition and the extent of viral maturity,[9−12] affect the fusion process and may play a regulatory or triggering role for some or all flaviviruses. The mechanism of fusion continues to be the subject of investigation, and the level of detail at which fusion mechanisms are conserved among flaviviruses is unknown.[13−15]

Mechanistic studies of Zika viral fusion thus have the potential to inform Zika biology as well as shed light on the degree of mechanistic conservation among flaviviruses. Critical questions include whether pH is sufficient to trigger fusion or merely one of several required factors, the pH range at which fusion occurs, and what other factors may be required for efficient fusion. Single-virus studies on the fusion of Zika virus to model membranes offer a means to probe these mechanisms in a controlled fashion and selectively reconstitute host components. Although there have been several receptors proposed for Zika virus (e.g., AXL), there is little consensus as to which, if any, is the key receptor for binding and what role it may play in triggering fusion.[16−20] While live-cell measurements can permit tracing of individual virions through the entry process, precise measurement of fusion conditions is challenging, and the ability to precisely perturb these conditions even more so. We and others have measured the fusion of infectious virus to synthetic target membranes, which permits exquisite control over the timing of fusion triggering, target membrane composition, and other soluble factors for fusion.[21−25] This approach enables richer mechanistic understanding, as evidenced by a

Received: July 24, 2018
Published: October 12, 2018

DOI: 10.1021/acscentsci.8b00494
ACS Cent. Sci. 2018, 4, 1503−1510

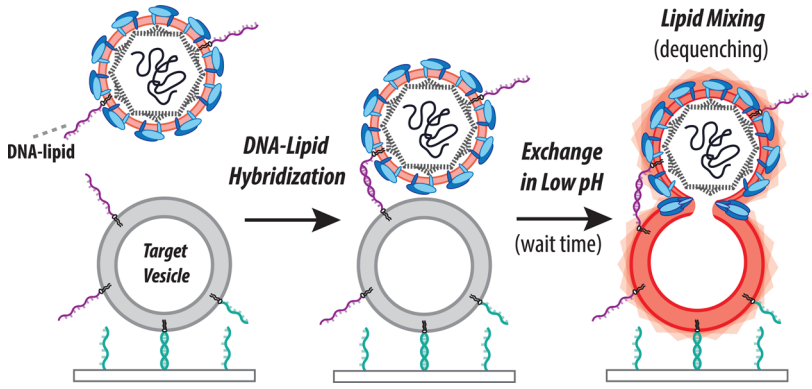

Figure 1. Schema of single virus fusion assay. Zika virus displays a low number of DNA–lipids and is fluorescently labeled with a self-quenched concentration of dye-labeled lipid (light pink). The target vesicles are tethered to a DNA-functionalized glass coverslip inside a microfluidic device by DNA–lipid hybridization (teal, sequence B–B′ orthogonal to purple DNA strands). Hybridization of viral and target DNA–lipids (purple, Sequence A–A′) binds the virus to the vesicle. Low pH buffer is exchanged into the microfluidic device to trigger fusion, which is observed by fluorescence dequenching due to lipid mixing between virus and target.

number of single virus binding and fusion studies, including West Nile virus.[21,26−29] Similarly, single-virus fusion kinetics yield a window into the fusion mechanism, in particular shedding light on mechanistic heterogeneity and the family of reactions required for fusion. This has been pursued fruitfully for other enveloped viruses[27,30−33] as well as nonviral systems.[34,35]

Here, we use an approach to single-virus measurement of Zika fusion that permits deconvolution of receptor/membrane binding from fusion. We have previously shown for influenza virus that tethering virions to target membranes using complementary DNA–lipid hybrids in the absence of native receptor can substitute for receptor binding.[30] In the case of influenza, where pH is the only trigger for fusion, we observed no measurable difference between the fusion (lipid mixing) kinetics of influenza bound by DNA–lipids or by its native receptor. We now leverage this approach to study the fusion of Zika virus, where a clear cellular receptor is not known. The driving hypothesis of our work is that if DNA–lipid tethering of Zika virus results in pH-triggered fusion, the fusion mechanisms will be at least informative of the mechanisms of fusion following receptor-mediated binding if not identical to those mechanisms. We show that fusion can indeed be triggered by pH alone and that negatively charged lipids are not required for Zika fusion. Our data suggest that if the pH range of fusion is considered alone, Zika virus hemifusion could occur in early endosomes and hemifusion efficiency would be further enhanced as the endosome matures. Additionally, we observe that while the efficiency of fusion is pH-sensitive, overall rates of fusion are relatively insensitive to pH (although there is a shift from rates at pH ∼6 to pH ∼5, which we discuss). We use kinetic modeling to analyze these results and demonstrate that an off-pathway state is required to reproduce our waiting-time distributions in any simple kinetic model. This off-pathway state represents one form of viral inactivation and is thus an important consideration for design and evaluation of fusion inhibitors.

RESULTS AND DISCUSSION

Single-virus measurements of Zika fusion kinetics via fluorescence microscopy require specifically labeled virus bound to target membranes. We performed this using virus labeled with a self-quenched concentration of Texas Red-DHPE bound to vesicles using DNA–lipid conjugates as schematized in Figure 1 and described in the Materials and Methods. Specific labeling was confirmed via immunofluorescence and immunoblotting (Figures S1 and S2); approximately 65% of fluorescently labeled particles were immunopositive for Zika E-protein. To examine the effect of labeling on viral integrity, labeled Zika virions were also confirmed via RT-qPCR to contain viral RNA (SI Appendix, Section 1.8), indicating that the labeling process did not grossly disrupt virions. Binding of labeled Zika virions to target vesicles immobilized within a microfluidic flow cell was highly specific, as negligible binding was observed when noncomplementary DNA sequences were used (Figure S4).

Single-virus Zika fusion kinetics were measured by triggering fusion using a low-pH buffer exchange over a 1−2 s interval, calibrated using pH-dependent fluorescence of target vesicles containing Oregon Green dye. For each labeled virion, the waiting time between pH drop and the onset of lipid mixing (a marker of hemifusion as lipid-conjugated dye is transferred from virus to vesicle and thus diluted) or, conversely, a failure to achieve lipid mixing was recorded. Representative images and fusion traces are shown in Figure 2. Waiting times for many virions were then compiled into a cumulative distribution function (CDF) (Figure 3A,B). The shape and time scale of the CDF contain information about the kinetically resolvable steps in the hemifusion process, which can be examined by kinetic modeling. CDFs are preferred over histograms to present waiting time data because they do not require binning time data, which can produce artifacts.[36]

To examine the role of pH in Zika virus fusion, we performed single virus lipid mixing experiments across a range of pH values designed to mimic endosomal pH values through most of the endocytic pathway (Figure 3A,B). We observed lipid mixing across the entire range of pH values tested, suggesting that the pH becomes permissive for Zika virions quite early during endosomal maturation and continues through late endosome to lysosome maturation. From pH 6.9 to pH 4.6, hemifusion efficiency increased approximately 3-fold in a roughly linear fashion (Figure 3A). The maximum efficiency of Zika virus lipid mixing is comparable to similar single virus fusion experiments with West Nile virus.[26] By way of comparison, dengue virus fusion largely occurs in late endosomes, although this may be determined by lipidic factors.[12,25,37] We hypothesize that negatively charged lipids, commonly found in late

DOI: 10.1021/acscentsci.8b00494
ACS Cent. Sci. 2018, 4, 1503−1510

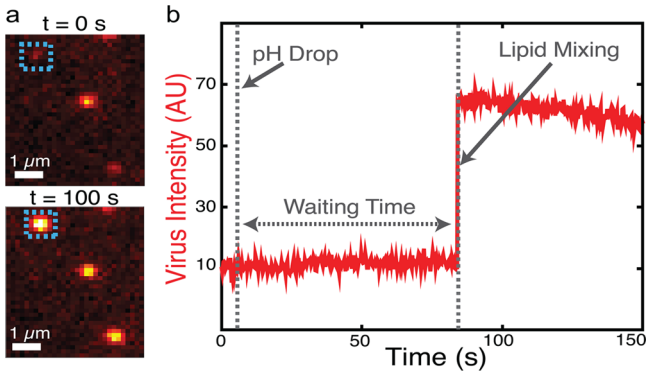

Figure 2. Single-virus fusion observed via fluorescence dequenching. (a) Example fluorescence micrographs of individual Zika virions (colored spots) bound to target vesicles (not visualized). At t = 0 (top) the virions' fluorescence is self-quenched but detectable as a dim spot. After low pH buffer exchange, 2 of 3 particles in the field of view exhibit dequenching due to lipid mixing after 100 s (bottom). (b) The fluorescence intensity trace of the virion boxed in A shows a sudden jump to higher fluorescence due to lipid mixing followed by photobleaching. The hemifusion wait time is defined as the time between pH drop and the onset of lipid mixing.

endosomes, function by either promoting viral attachment or enhancing an already fusion-competent virus; however, further work is necessary to explore the effect of lipid composition on fusion kinetics of Zika virus. While our data do not eliminate the possibility of additional cofactors regulating or enhancing Zika fusion within the endosome, low pH is sufficient to trigger lipid mixing events when Zika virus is bound to model membranes. We also observed a low (∼2−3%) efficiency of lipid mixing events at pH 7.4 that was significantly less than all lower pH values (p < 0.001 minimum) (Figure S6). This may suggest a low but nonzero probability of fusion at neutral pH if the virion is bound near a target membrane, which is further described in the Supporting Information (SI Appendix, section 2.1). As a control, when vesicles are tethered instead of virus, no fusion events are observed within the pH range of 7.4−4.6, and thus this behavior is specific to the presence of Zika virus.

In contrast to hemifusion efficiencies, hemifusion rates were relatively independent of pH (Figure 3B). Rates of lipid mixing increase slightly at lower pH values, but this effect was small compared to the magnitude of pH change: over a range where $[H^+]$ varied 200-fold, the $t_{1/2}$ for lipid mixing varied by no more than 2-fold. Therefore, while low pH is sufficient to trigger Zika virus, the rates of lipid mixing are largely insensitive to pH. Prior studies on other flaviviruses have shown that E-protein activation is pH sensitive.[26,38−43] Our data would indicate that such an activation step, although potentially pH-driven, is not rate-limiting for Zika fusion at pH < 5.8. As discussed below, this observation provides important constraints to the kinetic mechanism of fusion.

Kinetic Modeling of Zika Virus Hemifusion Data Suggests an Off-Pathway State. To analyze the mechanistic implications of our measurements of Zika hemifusion, we fit a series of kinetic models to the pH-dependent hemifusion data. We begin with simple models from chemical kinetics that assume well-mixed states with Markovian behavior; models that explicitly treat spatial patterns of fusion protein activation will be discussed later. These simple models assume that the underlying mechanism of fusion is conserved in pH-triggered fusion. It is apparent from gross examination of the waiting-time distributions (Figure 3) that overall lipid-mixing rates are roughly independent of pH at low pH but slower at high pH. This behavior requires at least two kinetic steps in a minimal model (1) a pH-independent step that is rate-limiting at low pH values, and (2) a pH-dependent step that is rate-limiting at higher pH values (5.8−7.4). This then leads to the following two-step minimal mechanism:

$$\mathrm{B} \underset{}{\overset{K_{BA}[H^+]}{\rightleftharpoons}} \mathrm{A} \xrightarrow{0.02\ s^{-1}} \mathrm{F} \qquad (1)$$

where B denotes bound virus, A denotes pH-activated virus in the membrane-bound state, and F denotes hemifused virus. For clarity we omit the state of the virus prior to membrane binding, as our experimental observation begins with virus bound to the target vesicle prior to pH drop. Therefore, we treat state B as the starting state of all viruses upon target binding. The final step leading to state F is treated as irreversible and is assigned as the pH-independent step. The pH-dependent step, state B to A, is treated as reversible, but $k_{AB} \ll k_{BA}[H^+]$ at all pH values tested, or a lag phase would have been observed in the CDF data. The pH-dependent transition has been postulated

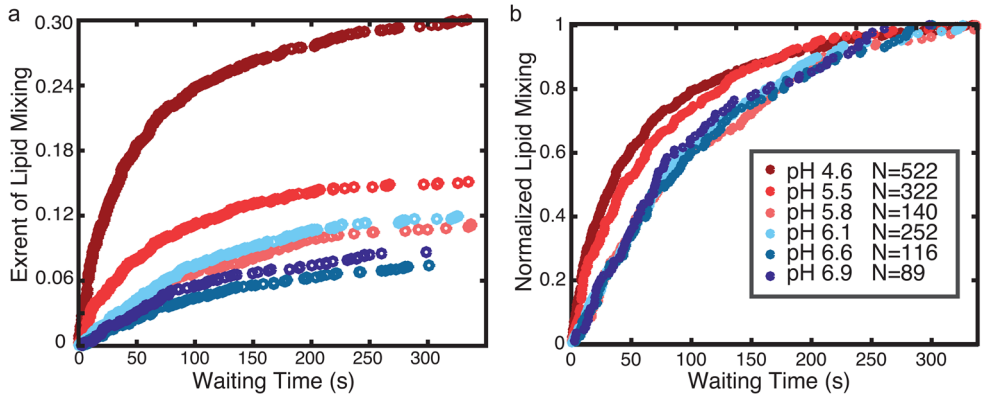

Figure 3. Zika virus hemifusion efficiency is sensitive to pH but rates are not. Plotted are cumulative distribution functions compiled from single-virus lipid-mixing wait times collected at different pH values and either normalized to fraction of total E-protein-positive particles (a) or normalized by the maximum observed fraction of lipid mixing at each pH value (b). Across the pH range, efficiency changes ∼3 fold: 333/1748 particles at pH 4.6, 145/1514 particles at pH 5.5, 95/1346 particles at pH 5.8, 186/2447 particles at pH 6.1, 68/1447 particles at pH 6.6, and 63/1145 particles at pH 6.9. Kinetic data were compiled from 29 independent fusion streams and replicated with an independent viral preparation. Fraction of total E-protein-positive particles was calculated using mean values measured via immunofluorescence assay (IFA) as described in Supporting Information.

DOI: 10.1021/acscentsci.8b00494
ACS Cent. Sci. 2018, 4, 1503−1510

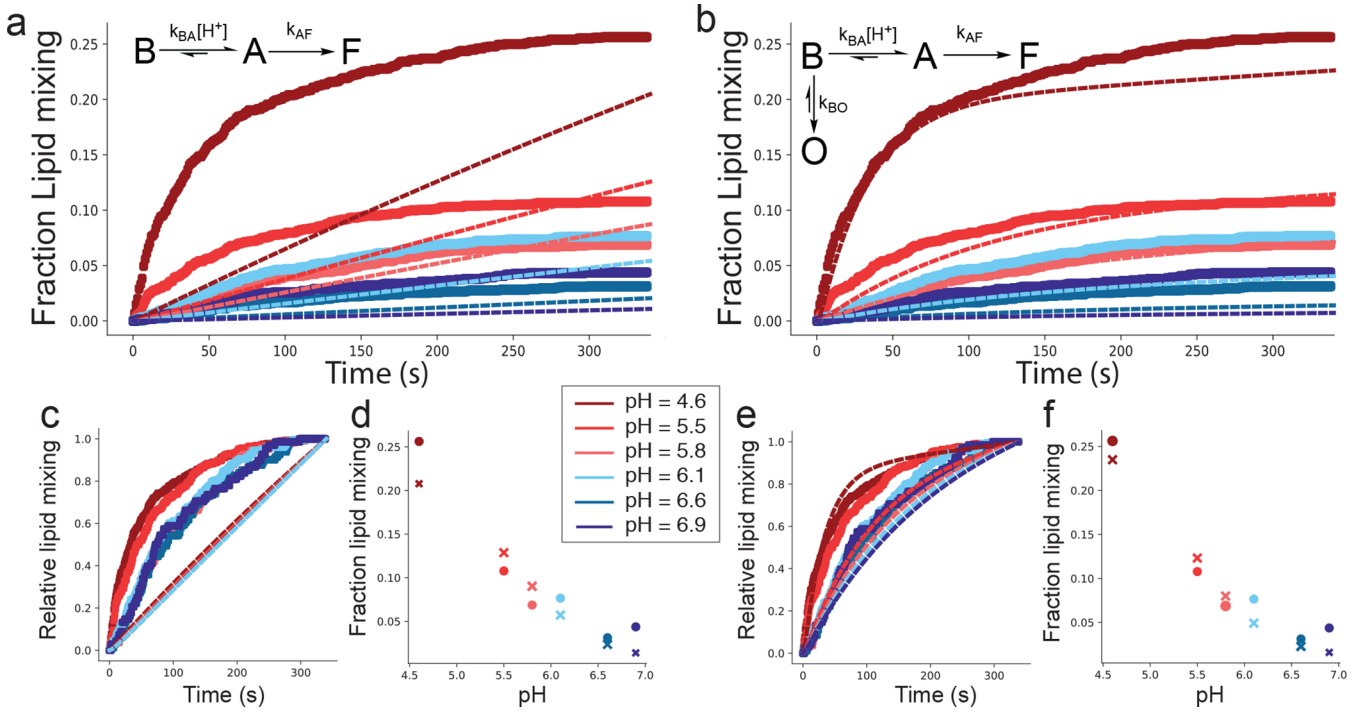

Figure 4. An off-pathway model is necessary to capture pH-dependent fusion kinetics. Plotted in panels A–B are lipid-mixing kinetic curves calculated from a linear model (a) and an off-pathway model (b) in thin lines, compared to observed single-virus fusion data at multiple pH values (thick lines). Kinetics are further visualized by normalizing all efficiencies to one (c and e for linear and off-pathway models), and efficiencies are estimated as the extent of lipid mixing at the end of the experiment (d, f). The linear model reproduces the lipid-mixing efficiency trends but does so at the expense of curve shape. The best-fit rate constants were $k_{BA} = 5.4 \times 10^4$ M^{-1} s^{-1}, $k_{BO} = 6.0 \times 10^{-3}$ s^{-1}, $k_{AB} = 0.29$ s^{-1}, $k_{AF} = 0.088$ s^{-1}, and $k_{OB} = 1.3 \times 10^{-4}$ s^{-1}.

to be related to the protonation of key histidines leading to a conformational shift.[40,43] The rate constant of the pH-independent step, k_{AF}, is estimated at 0.02 s^{-1} by approximating the CDF at pH 4.6 (where the pH-independent step should be rate-limiting) as a single exponential and solving the resulting equation.

This two-step mechanism can reasonably describe the hemifusion rates alone (Figure S7), but cannot successfully fit both rates and hemifusion efficiencies (Figure 4 and Figure S12). Indeed, any linear mechanism of this form cannot fit both the observed rates and efficiencies, even if additional states are added (compare Figure S12 and Figures S7–S9). A linear mechanism can only produce an efficiency less than one by generating kinetic curves that have not yet plateaued at the end of the experiment (Figure S12 and Figure S7). This agrees poorly with the observed CDFs as well as validation experiments where we extended the measurement window and did not measure a substantial increase in efficiency.

In order to capture both the observed rates and efficiency data, we found it necessary to include an off-pathway state in the reaction mechanism (eq 2). In this case, the on-pathway steps largely govern the rates, but partitioning between the on- and off-pathway states determines the final efficiencies.

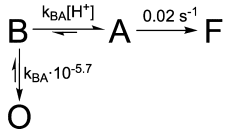

(2)

Rate constants for conversion to and from the off-pathway state O were estimated as follows. In this model, at pH values where k_{BA} $[H^+] \gg k_{BO}$, the relative efficiency approaches 1; conversely, when k_{BA} $[H^+] \ll k_{BO}$, the efficiency approaches 0. When the two are equal, the final efficiency is 0.5. By roughly treating our efficiency data (extents from Figure 3A) as linear with respect to pH, we estimated the off-pathway state should be half populated around pH 5.7 (Figure S11). Consequently, we set $k_{BO} = k_{BA} \times 10^{-5.7}$. Because our efficiency data is pH-dependent, the off-pathway state must occur in competition with the pH-dependent step; otherwise no pH dependence would be observed. For the same reason, transition rates to the off-pathway state also cannot be first-order with respect to $[H^+]$. Our initial analyses approximate conversion to the off-pathway state as irreversible; however this model does not rule out possibility for a slow return from the off-pathway state. Indeed, unconstrained fits presented in Figure 4 show $0 < k_{OB} \ll k_{BO}$. As noted above, state B is assumed to be the starting state of the model following virus binding. The off-pathway state depends on close proximity to a target membrane; otherwise, the native state of the virus prior to membrane binding would largely be in this off-pathway state and fusion would not be observed.

Using the model in eq 2, we performed a one parameter fit to our lipid mixing data, only allowing k_{BA} to vary (Figure S12). Despite the simplified nature of this model, we found better agreement with the general features of our data—pH-dependent efficiencies with only minimal change in hemifusion rates.

However, the lipid mixing efficiencies obtained via this model were essentially linear with respect to pH and approached zero at high pH. In contrast, the observed efficiencies approached a limiting value of 2–3% at pH 7.4. As low pH has been shown to be necessary for efficient infection by Zika virus,[44] we further concentrated on the pH-dependent lipid mixing process and corrected the cumulative distribution functions at all

DOI: 10.1021/acscentsci.8b00494
ACS Cent. Sci. 2018, 4, 1503–1510

other pH values by subtracting the pH 7.4 CDF (Figure S13). Using these corrected lipid-mixing curves, we performed fits of the models in eqs 1 and 2, allowing all parameters to vary freely fitting all pH values simultaneously. We observed that an off-pathway model was still required (Figure 4) and that the background subtraction improved the fitted efficiencies (compare Figure S12 and Figure 4). This suggests that an off-pathway state is required to fit our lipid mixing data with any simple kinetic model.

Cellular Automaton Models of Fusion Kinetics. Because many viral fusion processes are known to require multiple fusion proteins, cellular automaton models have been developed to incorporate protein spatial arrangement and activation into the analysis of single-virus fusion traces.[26,33,45] These models also incorporate structural and biochemical information to hypothesize the molecular identities of intermediate states in the kinetic schemes employed. We therefore implemented a cellular automaton model that was previously used to analyze West Nile virus fusion,[26] consisting of four structural states in a linear reaction scheme, and used it to analyze our pH-dependent Zika virus fusion data in a fashion analogous to the simpler models above.

To determine whether the geometrical constraints in the simulation model could compensate for the requirement of an off-pathway state in the simple kinetic model (eq 2), we implemented a number of kinetic schemes within the cellular automaton framework and fit them to our data. Parameterization of the model is described in the Supporting Information (SI Appendix, Section S.3) and was performed analogously to that previously reported for West Nile virus, but with careful treatment of pH pre-equilibration for multi-pH experiments. None of the linear models tested were able to fit the Zika virus fusion data (Figures S14 and S15). However, addition of an off-pathway state in the cellular automaton model (Figure S15) analogous to eq 2 above resulted in a fit approximately similar in quality to the best-fit parameters for eq 2. Whether a simple or more complex kinetic scheme is used, we conclude that an off-pathway state is needed to capture both the efficiency and rates of Zika virus hemifusion as pH is varied.

According to the structural hypotheses encoded in prior models of West Nile virus,[26] our related model for Zika suggests that E-protein monomers could adopt an off-pathway conformation following insertion into the target membrane. This transition is either slowly reversible or irreversible on the time-scales of fusion. There are currently insufficient biochemical data on Zika virus to definitively assign structural identities to the states in our model, so this remains speculation. If we accept prior biochemical analyses and hypotheses regarding related viruses, this off-pathway state would be closely related to viral inactivation, although our model requires the off-pathway state to depend on the presence of target membranes and thus may be distinct from additional slow inactivation of flaviviruses in solution.[46,47]

Finally, we note that both the simple kinetic and cellular automaton models have a similar categorical shortcoming: They both predict that lipid-mixing efficiency should be very sensitive to the time delay between virus binding to the target membrane and pH drop, which we do not observe. In our experimental data, viruses bound to target membranes showed similar kinetic behavior whether bound for <10 or >20 min prior to the pH drop (Figure S16). This indicates that, although an off-pathway state is required, neither model is complete, and suggests an avenue for follow-up investigation.

CONCLUSION

Using DNA−lipids as surrogate viral receptors permits the study of Zika virus fusion mechanisms distinct from viral binding and even without definitive identification of the natural receptor. Measuring single-virus fusion events in this manner, we have established that pH is sufficient to trigger fusion of prebound virus to synthetic target membranes. Viral hemifusion can occur in a pH range consistent with early endosomes but increases in efficiency at lower pH values. This suggests that the pH of late endosomes and lysosomes is also compatible with Zika viral fusion, although other factors in different endocytic compartments such as lipid composition changes and protease activity may act to promote or inhibit fusion in different compartments. Prior work has tracked dengue and West Nile virions trafficking in live cells and proposed that those viruses fuse in late endosomes,[12,25,37,48] and this is likely the case for Zika as well.

Strikingly, the rates of Zika hemifusion were largely insensitive to pH, suggesting that the rate-limiting step of hemifusion must be pH-independent below approximately pH 6. This finding implies that conformational extension of the viral E-protein to permit fusion, demonstrated to be a pH-dependent process for closely related flaviviruses,[26,38,49,50] is not rate-limiting in this pH range. We have deliberately avoided assigning specific structural features to states in our kinetic models, but our modified implementation of prior cellular automaton models used for West Nile data to fit Zika viral fusion kinetics raises the hypothesis that the off-pathway state we detect in Zika fusion may occur after E-protein extension and insertion into the target membrane. Speculatively, this could represent an aggregation, misfolding, or similar state of the E-protein which contributes to inactivation.

In addition to low pH, other factors have been implicated in regulating flavivirus fusion, including endosomal lipid composition, temperature, and extent of viral maturation.[9,12] Our results suggest that pH is sufficient to trigger Zika virus fusion, but they do not exclude the possibility of other endosomal factors influencing the fusion process or enhancing fusion efficiency. Our single virus fusion platform enables future examination of how these and other factors affect Zika virus fusion. We anticipate that this platform using DNA−lipids as surrogate receptors will also facilitate the study of single-virus fusion by other enveloped viruses with unknown or difficult-to-isolate native receptors.

MATERIALS AND METHODS

Materials. Dioleoylphosphatidylethanolamine (DOPE), palmitoyl oleoylphosphatidylcholine (POPC), and cholesterol were purchased from Avanti Polar Lipids (Alabaster, AL). Texas Red-1,2-dihexadecanoyl-*sn*-glycero-3-phosphoethanolamine (TR-DHPE), Oregon Green-1,2-dihexadecanoyl-*sn*-glycero-3-phosphoethanolamine (OG-DHPE), goat anti-mouse IgG (H + L) secondary antibody, Alexa Fluor 488 and anti-flavivirus group antigen, and clone: D1-4G2-4-15, EMD Millipore were purchased from Thermo Fisher Scientific (Waltham, MA). IRDye 680RD goat anti-mouse IgG (H + L) 0.5 mg/mL was generously supplied by the Bertozzi lab (Stanford University). PCR primers were ordered from the Stanford PAN Facility, (SI Appendix, Table S2). Chloroform, methanol, and buffer salts were obtained from Fisher Scientific (Pittsburgh, PA) and Sigma-Aldrich (St. Louis, MO). 11-Azidoundecyltrimethoxysilane was obtained from Sikemia (Clapiers, France).

DOI: 10.1021/acscentsci.8b00494
ACS Cent. Sci. 2018, 4, 1503−1510

Polydimethylsiloxane (PDMS) was obtained from Ellsworth Adhesives (Hayward, CA). Tridecafluoro-1,1,2,2-tetrahydrooctyltrichlorosilane was obtained from Gelest (Morrisville, PA). 1,1′,1″-Tris(1*H*-1,2,3-triazol-4-yl-1-acetic acid ethyl ester) trimethylamine (TTMA) ligand was a generous gift from Professor Christopher Chidsey at Stanford University. Ethynyl phosphonic acid was synthesized as previously described.[51] Zika virus is a BSL-2 agent and was handled following an approved administrative biosafety panel protocol at Stanford University. No other unexpected or unusually high safety hazards were encountered with this work.

Buffers. The following buffers were used. Reaction buffer (RB) = 10 mM NaH_2PO_4, 90 mM sodium citrate, 150 mM NaCl, pH 7.4. Fusion buffer (FB) = 10 mM NaH_2PO_4, 90 mM sodium citrate, 150 mM NaCl, pH as indicated. HB buffer = 20 mM Hepes, 150 mM NaCl, pH 7.2. sucrose cushion = 20% m/v sucrose, 20 mM Hepes, 150 mM NaCl, pH 7.3. We found it necessary to charcoal filter our sucrose solutions, which contained contaminant green fluorescence present from the manufacturer and which otherwise made it impossible to perform our single-molecule DNA−lipid incorporation measurements. As a cautionary note to other researchers, this charcoal filtration can substantially alter the pH of the sucrose cushion, unless it is appropriately buffered.

Microscopy. All epifluorescence micrographs and videos were acquired with a Nikon Ti-U microscope using a 100× oil immersion objective, NA = 1.49 (Nikon Instruments, Melville, NY), with a Spectra-X LED Light Engine (Lumencor, Beaverton, OR) as an excitation light source, and additional excitation/emission filter wheels (SI Appendix, Supporting Methods S1.9). Images were recorded with an Andor iXon 897 EMCCD camera (Andor Technologies, Belfast, UK) using 16-bit image settings and were captured with Metamorph software (Molecular Devices, Sunnyvale, CA). See Supporting Information (SI Appendix) for additional microscope details.

Viral Growth. Zika Virus (DAKAR41524) was grown in Vero cells according to an adaptation of a standard protocol for dengue virus.[52] Cells at approximately 80% confluence were inoculated at a multiplicity of infection of approximately 0.05, grown in DMEM media with 2% fetal bovine serum, and the supernatant was harvested at 96 and 120 h after incubation in a tissue culture incubator at 37 °C, 5% CO_2. Gross cellular debris was removed by centrifugation at 4000 rcf, 4 °C for 10 min, and the sample was concentrated 20× by centrifugation in 30 kDa-cutoff spin concentrators and frozen at −80 °C until purification. We observed that this protocol maintained viral infectivity better than freezing unconcentrated supernatant in 23% fetal bovine serum until purification.

Viral Purification and Labeling. Zika virus was thawed on ice overnight before ultracentrifugation through a 20% sucrose cushion at 100000*g* for 3 h at 4 °C. The supernatant was discarded, and the pellet was resuspended by extensive pipetting in 100 μL of HB. To prepare the dye labeling solution, a 400 μL solution of 13.5 μM Tx-Red DHPE in HB with 2.5% ethanol was sonicated at 55 °C for 20 min then cooled to room temperature. We found it necessary to heat/sonicate the dye labeling solution prior to virus addition. This dispersed dye aggregates that would otherwise be copurified with viral particles. The resuspended virus was added to the dye solution (yielding a 10 μM Tx-Red DHPE solution) and gently rocked at 25 °C for 2 h. To purify away free dye, the labeled virus mixture underwent ultracentrifugation through a 20% sucrose cushion at 100000*g* for 3 h at 4 °C. The pellet was resuspended in fresh 100 μL HB. This labeled virus suspension was stored at 4 °C and used in lipid mixing assays within several days. A self-quenching concentration of dye is required to accurately quantitate lipid mixing between virus and 100 nm vesicles. This labeling procedure is similar to those we and others have used to label other enveloped viruses, and the dye concentrations used in these experiments are lower than those previously found not to perturb West Nile and Kunjin virus infectivity.[26] Additionally, a 2-fold increase in the TR-DHPE dye added did not alter the measured lipid-mixing efficiency (Figure S5).

DNA−Lipid Incorporation into Zika Virions. The number of fluorescently labeled particles was estimated by adsorption of a fixed volume of viral suspension to a cleaned glass coverslip and counted using fluorescence microscopy. DNA−lipids were added at a ratio of 10 μM DNA−lipid to an estimated 1 pM of viral particles and allowed to incubate for 30 min at 24 °C to ensure all virions incorporated DNA−lipid. Single-step photobleaching was performed on particles with DNA−lipids conjugated to Alexa 488 (Sequence X, Table S1) to determine the number of DNA−lipids incorporated into each particle. The median number of DNA−lipids per virion was two (Figure S3). DNA sequence A and A′ were utilized for viral binding and fusion because they increased tethering speed and density of bound virions per field of view (FOV). The increased binding speed of DNA sequence A and A′ as compared to B and B′ is likely a result of the former being a non-fully overlapping sequence, which leads to faster tethering as characterized in earlier work.[34]

Lipid-Mixing Assay. Lipid-mixing assays were performed as previously described[30] and (Figure 1). In brief, target membranes, ∼100 nm diameter lipid vesicles displaying DNA−lipid sequences A′ and B (SI Table 1), were tethered to glass slides functionalized with sequence B′ inside of a microfluidic flow cell in the presence of RB. Excess vesicles were rinsed from the flow cell with RB. An estimated 10 pmol of labeled virions containing DNA-lipid sequence A was added to the flow cell, and the cell was then rinsed with RB after 2−5 min to remove excess unbound virus. Fluorescence microscopy was used to collect a stream of images for 1200 frames at a frame rate of 3.47 frames/s. After the start of the stream, low pH buffer (FB pH 4.6−6.9) was immediately exchanged into the chamber and the flow was started. Vesicles with a pH indicator (2 mol % OG-DHPE) were used to calibrate the exchange time of the low pH buffer (FB pH 5.1) (1−2 s).[30] The time between introduction of low pH to the field of view (FOV) and dequenching events was then analyzed using Matlab (source code available from https://github.com/kassonlab).

Kinetic Modeling. Construction and fitting of kinetic models to the lipid mixing data were performed using Matlab and Python code available from https://github.com/kassonlab. For each kinetic model, matrix exponentials were used to solve the system of coupled ordinary differential equations and calculate the fraction of virions that have undergone lipid mixing at discrete time points between 0 and 340 s, corresponding to the cumulative distribution function (CDF) curves compiled from our experimental data at each waiting time after pH drop (t = 0). Additionally, to account for the time period between virus binding to target vesicles and pH drop (∼10 min), the kinetic model was run for 10 min at pH 7.4, and this was used as the starting state at t = 0. All viruses were defined to be in the first state at t = −10 min (State B in the scheme shown in eq 2).

DOI: 10.1021/acscentsci.8b00494
ACS Cent. Sci. 2018, 4, 1503−1510

Kinetic model parameters were fit to the data across all pH values simultaneously using a maximum-likelihood procedure as follows. The probability density function (PDF) for lipid mixing at a particular pH is expressed as

$$f(x;\, k,\, \mathrm{pH}) = \begin{cases} \pi(k,\, \mathrm{pH}) f_{\mathrm{hemi}}(x;\, k,\, \mathrm{pH}) & x_{\mathrm{hemi}} \\ 1 - \pi(k,\, \mathrm{pH}) & x_{\mathrm{not}} \end{cases} \quad (3)$$

where k is the set of rate constants in the model, π is the hemifusion efficiency, x_{hemi} is the hemifusion wait time of a virus that underwent lipid mixing, x_{not} is a virus observed not to undergo lipid mixing, and f_{hemi} is the PDF of hemifusion wait times. f_{hemi} was calculated as the numerical derivative of the solution to the kinetic master equation. This then leads to the log likelihood expression:

$$\log L\,(x;\, k,\, \mathrm{pH}) = \sum_{x} (\log f(x_{\mathrm{hemi}};\, k,\, \mathrm{pH})) + N_{\mathrm{hemi}} \log \pi(k,\, \mathrm{pH}) + N_{\mathrm{not}} \log(1 - \pi(k,\, \mathrm{pH})) \quad (4)$$

where x_{hemi} is the experimentally observed wait time of an individual virus, N_{hemi} is the number of viruses experimentally observed to undergo lipid mixing, and N_{not} is the number of viruses that did not undergo lipid mixing. Fitting is then performed by minimizing the negative log likelihood expression across all experimentally measured pH values, written as

$$\mathrm{NLL}\,(k) = -\sum_{\mathrm{pH}} \frac{\log L}{N_{\mathrm{tot}}} \quad (5)$$

where N_{tot} is the total number of viruses analyzed at a particular pH value.

■ ASSOCIATED CONTENT

Supporting Information

The Supporting Information is available free of charge on the ACS Publications website at DOI: 10.1021/acscentsci.8b00494.

Additional experimental methods, DNA sequences, PCR primers, additional microscopy information, detailed implementation of kinetic models, additional validation of viral labeling and DNA insertion, and additional kinetic models (PDF)

■ AUTHOR INFORMATION

Corresponding Authors

*(S.G.B.) E-mail: sboxer@stanford.edu. Address: 380 Roth Way, Stanford CA 94305-5012. Phone: 650-723-4442.
*(P.M.K.) E-mail: kasson@virginia.edu.

ORCID

Robert J. Rawle: 0000-0003-4958-4919
Elizabeth R. Webster: 0000-0003-2764-1118
Peter M. Kasson: 0000-0002-3111-8103
Steven G. Boxer: 0000-0001-9167-4286

Author Contributions

#R.J.R. and E.R.W. made an equal contribution.

Author Contributions

E.R.W. and R.J.R. designed experiments, performed experiments, analyzed data, and wrote the paper. R.J.R. and P.M.K. wrote Matlab and Python code used in the modeling and analysis. M.J. and P.M.K. grew and harvested the virus. P.M.K. and S.G.B. designed experiments, analyzed data, and wrote the paper.

Notes

The authors declare no competing financial interest.

■ ACKNOWLEDGMENTS

This work was supported by a University of Virginia Research Development Award and a Wallenberg Academy Fellowship to P.M.K. and National Institutes of Health Grant R35 GM118044 to S.G.B. E.R.W. was supported by an NSF predoctoral fellowship and from the Stanford ChEM-H Chemistry/Biology Interface Predoctoral Training Program. The authors thank Isabel Goronzy (Stanford) for designing and performing the RT-qPCR measurements and Stephen Harrison and Luke Chao for helpful discussions on kinetic modeling.

■ REFERENCES

(1) Larocca, R. A.; Abbink, P.; Peron, J. P. S.; Zanotto, P. M. de A.; lampietro, M. J.; Badamchi-Zadeh, A.; Boyd, M.; Ng'ang'a, D.; Kirilova, M.; Nityanandam, R.; et al. Vaccine protection against zika virus from brazil. *Nature* **2016**, *536*, 474−478.

(2) Sapparapu, G.; Fernandez, E.; Kose, N.; Cao, B.; Fox, J. M.; Bombardi, R. G.; Zhao, H.; Nelson, C. A.; Bryan, A. L.; Barnes, T.; et al. Neutralizing human antibodies prevent zika virus replication and fetal disease in mice. *Nature* **2016**, *540*, 443−447.

(3) Haddow, A. D.; Schuh, A. J.; Yasuda, C. Y.; Kasper, M. R.; Heang, V.; Huy, R.; Guzman, H.; Tesh, R. B.; Weaver, S. C. Genetic characterization of zika virus strains: geographic expansion of the Asian lineage. *PLoS Neglected Trop. Dis.* **2012**, *6*, No. e1477.

(4) Shan, C.; Muruato, A. E.; Jagger, B. W.; Richner, J.; Nunes, B. T. D.; Medeiros, D. B. A.; Xie, X.; Nunes, J. G. C.; Morabito, K. M.; Kong, W.-P.; et al. A single-dose live-attenuated vaccine prevents zika virus pregnancy transmission and testis damage. *Nat. Commun.* **2017**, *8*, 676.

(5) Nour, A. M.; Li, Y.; Wolenski, J.; Modis, Y. Viral membrane fusion and nucleocapsid delivery into the cytoplasm are distinct events in some flaviviruses. *PLoS Pathog.* **2013**, *9*, e1003585.

(6) Espósito, D. L. A.; Nguyen, J. B.; DeWitt, D. C.; Rhoades, E.; Modis, Y. Physico-chemical requirements and kinetics of membrane fusion of flavivirus-like particles. *J. Gen. Virol.* **2015**, *96*, 1702−1711.

(7) Gollins, S. W.; Porterfield, J. S. PH-dependent fusion between the flavivirus west nile and liposomal model membranes. *J. Gen. Virol.* **1986**, *67*, 157−166.

(8) Modis, Y.; Ogata, S.; Clements, D.; Harrison, S. C. Structure of the dengue virus envelope protein after membrane fusion. *Nature* **2004**, *427*, 313−319.

(9) Mukherjee, S.; Sirohi, D.; Dowd, K.; Chen, Z.; Diamond, M.; Kuhn, R.; Pierson, T. C. Enhancing dengue virus maturation using a stable furin over-expressing cell line. *Virology* **2016**, *497*, 33−40.

(10) Kostyuchenko, V. A.; Zhang, Q.; Tan, J. L.; Ng, T.-S.; Lok, S.-M. Immature and mature dengue serotype 1 virus structures provide insight into the maturation process. *J. Virol.* **2013**, *87*, 7700−7707.

(11) Dowd, K. a; Mukherjee, S.; Kuhn, R. J.; Pierson, T. C. Combined effects of the structural heterogeneity and dynamics of flaviviruses on antibody recognition. *J. Virol.* **2014**, *88*, 11726−11737.

(12) Zaitseva, E.; Yang, S.-T.; Melikov, K.; Pourmal, S.; Chernomordik, L. V. Dengue virus ensures its fusion in late endosomes using compartment-specific lipids. *PLoS Pathog.* **2010**, *6*, e1001131.

(13) Bressanelli, S.; Stiasny, K.; Allison, S. L.; Stura, E. A.; Duquerroy, S.; Lescar, J.; Heinz, F. X.; Rey, A. Structure of a flavivirus envelope glycoprotein in its low-ph-induced membrane fusion conformation. *EMBO J.* **2004**, *23*, 728−738.

(14) Kanai, R.; Kar, K.; Anthony, K.; Gould, L. H.; Ledizet, M.; Fikrig, E.; Marasco, W. A.; Koski, R. A.; Modis, Y. Crystal structure of west nile virus envelope glycoprotein reveals viral surface epitopes. *J. Virol.* **2006**, *80*, 11000−11008.

DOI: 10.1021/acscentsci.8b00494
ACS Cent. Sci. 2018, 4, 1503−1510

(15) Kuhn, R. J.; Zhang, W.; Rossmann, M. G.; Pletnev, S. V.; Corver, J.; Lenches, E.; Jones, C. T.; Mukhopadhyay, S.; Chipman, P. R.; Strauss, E. G.; et al. Structure of dengue virus: implications for flavivirus organization, maturation, and fusion. *Cell* **2002**, *108*, 717−725.
(16) Richard, A. S.; Shim, B.-S.; Kwon, Y.-C.; Zhang, R.; Otsuka, Y.; Schmitt, K.; Berri, F.; Diamond, M. S.; Choe, H. AXL-dependent infection of human fetal endothelial cells distinguishes zika virus from other pathogenic flaviviruses. *Proc. Natl. Acad. Sci. U. S. A.* **2017**, *114*, 2024−2029.
(17) Nowakowski, T. J.; Pollen, A. A.; Di Lullo, E.; Sandoval-Espinosa, C.; Bershteyn, M.; Kriegstein, A. R.; Wu, X.; Lemke, G.; Lu, Q.; Picone, O.; et al. Expression analysis highlights axl as a candidate zika virus entry receptor in neural stem cells. *Cell Stem Cell* **2016**, *18*, 591−596.
(18) Hamel, R.; Dejarnac, O.; Wichit, S.; Ekchariyawat, P.; Neyret, A.; Luplertlop, N.; Perera-Lecoin, M.; Surasombatpattana, P.; Talignani, L.; Thomas, F.; et al. Biology of zika virus infection in human skin cells. *J. Virol.* **2015**, *89*, 8880−8896.
(19) Harrison, S. C. Immunogenic cross-talk between dengue and zika viruses. *Nat. Immunol.* **2016**, *17*, 1010−1012.
(20) Moller-Tank, S.; Kondratowicz, A. S.; Davey, R. A.; Rennert, P. D.; Maury, W. Role of the phosphatidylserine receptor tim-1 in enveloped-virus entry. *J. Virol.* **2013**, *87*, 8327−8341.
(21) Melikyan, G. B.; Barnard, R. J. O.; Abrahamyan, L. G.; Mothes, W.; Young, J. A. T. Imaging individual retroviral fusion events: from hemifusion to pore formation and growth. *Proc. Natl. Acad. Sci. U. S. A.* **2005**, *102*, 8728−8733.
(22) Matos, P. M.; Marin, M.; Ahn, B.; Lam, W.; Santos, N. C.; Melikyan, G. B. Anionic lipids are required for vesicular stomatitis virus g protein-mediated single particle fusion with supported lipid bilayers. *J. Biol. Chem.* **2013**, *288*, 12416−12425.
(23) Zaitseva, E.; Zaitsev, E.; Melikov, K.; Arakelyan, A.; Marin, M.; Villasmil, R.; Margolis, L. B.; Melikyan, G. B.; Chernomordik, L. V. Fusion stage of hiv-1 entry depends on virus-induced cell surface exposure of phosphatidylserine. *Cell Host Microbe* **2017**, *22*, 99−110.
(24) Lakadamyali, M.; Rust, M. J.; Babcock, H. P.; Zhuang, X. Visualizing infection of individual influenza viruses. *Proc. Natl. Acad. Sci. U. S. A.* **2003**, *100*, 9280−8285.
(25) Van Der Schaar, H. M.; Rust, M. J.; Chen, C.; Van Der Ende-Metselaar, H.; Wilschut, J.; Zhuang, X.; Smit, J. M. Dissecting the cell entry pathway of dengue virus by single-particle tracking in living cells. *PLoS Pathog.* **2008**, *4*, No. e1000244.
(26) Chao, L. H.; Klein, D. E.; Schmidt, A. G.; Peña, J. M.; Harrison, S. C. Sequential conformational rearrangements in flavivirus membrane fusion. *eLife* **2014**, *3*, No. e04389, DOI: 10.7554/eLife.04389.
(27) Floyd, D. L.; Ragains, J. R.; Skehel, J. J.; Harrison, S. C.; van Oijen, A. M. Single-particle kinetics of influenza virus membrane fusion. *Proc. Natl. Acad. Sci. U. S. A.* **2008**, *105*, 15382−15387.
(28) Wessels, L.; Elting, M. W.; Scimeca, D.; Weninger, K. Rapid membrane fusion of individual virus particles with supported lipid bilayers. *Biophys. J.* **2007**, *93*, 526−538.
(29) Costello, D. A.; Lee, D. W.; Drewes, J.; Vasquez, K. A.; Kisler, K.; Wiesner, U.; Pollack, L.; Whittaker, G. R.; Daniel, S. Influenza virus-membrane fusion triggered by proton uncaging for single particle studies of fusion kinetics. *Anal. Chem.* **2012**, *84*, 8480−8489.
(30) Rawle, R. J.; Boxer, S. G.; Kasson, P. M. Disentangling viral membrane fusion from receptor binding using synthetic dna-lipid conjugates. *Biophys. J.* **2016**, *111*, 123−131.
(31) Harrison, S. C. Viral membrane fusion. *Virology* **2015**, *479−480*, 498−507.
(32) Hsu, H.-L.; Millet, J. K.; Costello, D. A.; Whittaker, G. R.; Daniel, S.; Sandman, P. M.; Lanard, J.; Taubenberger, J. K.; Morens, D. M.; Dawood, F. S.; et al. Viral fusion efficacy of specific h3n2 influenza virus reassortant combinations at single-particle level. *Sci. Rep.* **2016**, *6*, 35537.
(33) Kim, I. S.; Jenni, S.; Stanifer, M. L.; Roth, E.; Whelan, S. P. J.; Van Oijen, A. M.; Harrison, S. C. Mechanism of membrane fusion induced by vesicular stomatitis virus G protein. *Proc. Natl. Acad. Sci. U. S. A.* **2017**, *114*, E28−E36.
(34) Chan, Y.-H. M.; Lenz, P.; Boxer, S. G. Kinetics of dna-mediated docking reactions between vesicles tethered to supported lipid bilayers. *Proc. Natl. Acad. Sci. U. S. A.* **2007**, *104*, 18913−18918.
(35) Kyoung, M.; Zhang, Y.; Diao, J.; Chu, S.; Brunger, A. T. Studying calcium-triggered vesicle fusion in a single vesicle-vesicle content and lipid-mixing system. *Nat. Protoc.* **2012**, *8*, 1−16.
(36) Massey, F. J. The kolmogorov-smirnov test for goodness of fit. *J. Am. Stat. Assoc.* **1951**, *46*, 68−78.
(37) Chu, J. J. H.; Ng, M. L. Infectious entry of west nile virus occurs through a clathrin-mediated endocytic pathway. *J. Virol.* **2004**, *78*, 10543−10555.
(38) Zheng, A.; Yuan, F.; Kleinfelter, L. M.; Kielian, M. A toggle switch controls the low ph-triggered rearrangement and maturation of the dengue virus envelope proteins. *Nat. Commun.* **2014**, *5*, 3877.
(39) Zhang, X.; Sheng, J.; Austin, S. K.; Hoornweg, T. E.; Smit, J. M.; Kuhn, R. J.; Diamond, M. S.; Rossmann, M. G. Structure of acidic ph dengue virus showing the fusogenic glycoprotein trimers. *J. Virol.* **2015**, *89*, 743−750.
(40) Fritz, R.; Stiasny, K.; Heinz, F. Identification of specific histidine residues as ph sensors in flavivirus membrane fusion. *J. Cell Biol.* **2008***183*, 353−361,.
(41) White, J. M.; Delos, S. E.; Brecher, M.; Schornberg, K. Structures and mechanisms of viral membrane fusion proteins: multiple variations on a common theme. *Crit. Rev. Biochem. Mol. Biol.* **2008**, *43*, 189−219.
(42) Yang, S.-T.; Zaitseva, E.; Chernomordik, L. V.; Melikov, K. Cell-penetrating peptide induces leaky fusion of liposomes containing late endosome-specific anionic lipid. *Biophys. J.* **2010**, *99*, 2525−2533.
(43) Stiasny, K.; Fritz, R.; Pangerl, K.; Heinz, F. X. Molecular mechanisms of flavivirus membrane fusion. *Amino Acids* **2011**, *41*, 1159−1163.
(44) Persaud, M.; Martinez-Lopez, A.; Buffone, C.; Porcelli, S. A.; Diaz-Griffero, F. Infection by zika viruses requires the transmembrane protein axl, endocytosis and low ph. *Virology* **2018**, *518*, 301−312.
(45) Ivanovic, T.; Choi, J. L.; Whelan, S. P.; Van Oijen, A. M.; Harrison, S. C. Influenza-virus membrane fusion by cooperative fold-back of stochastically induced hemagglutinin intermediates. *eLife* **2013**, *2*, DOI: 10.7554/eLife.00333.
(46) Sirohi, D.; Kuhn, R. J. Zika virus structure, maturation, and receptors. *J. Infect. Dis.* **2017**, *216*, S935−S944.
(47) Kuhn, R. J.; Dowd, K. A.; Beth Post, C.; Pierson, T. C. Shake, rattle, and roll: impact of the dynamics of flavivirus particles on their interactions with the host. *Virology* **2015**, *479−480*, 508−517.
(48) White, J. M.; Whittaker, G. R. Fusion of enveloped viruses in endosomes. *Traffic* **2016**, *17*, 593−614.
(49) Zhang, S.; Kostyuchenko, V. A.; Ng, T.-S.; Lim, X.-N.; Ooi, J. S. G.; Lambert, S.; Tan, T. Y.; Widman, D. G.; Shi, J.; Baric, R. S. Neutralization mechanism of a highly potent antibody against zika virus. *Nat. Commun.* **2016**, *7*, 13679.
(50) Klein, D. E.; Choi, J. L.; Harrison, S. C. Structure of a dengue virus envelope protein late-stage fusion intermediate. *J. Virol.* **2013**, *87*, 2287−2293.
(51) Hughes, L. D. Model membrane architectures for the study of membrane proteins. Doctoral Dissertation, Stanford University, **2013**. https://purl.stanford.edu/xr495nv6897. Accessed July 20, 2018.
(52) Medina, F.; Medina, J. F.; Colón, C.; Vergne, E.; Santiago, G. A.; Muñoz-Jordán, J. L. Dengue virus: isolation, propagation, quantification, and storage. *Curr. Protoc. Microbiol.* **2012**, *27*, 15D.2.1−15D.2.24.

DOI: 10.1021/acscentsci.8b00494
ACS Cent. Sci. 2018, 4, 1503−1510